Conolysin-Mt: A *Conus* Peptide That Disrupts Cellular Membranes[†]

Jason S. Biggs,[‡,§] Yosef Rosenfeld,[§,‖] Yechiel Shai,[‖] and B. M. Olivera*,[‡]

Department of Biology, University of Utah, Salt Lake City, Utah 84108, and Biological Chemistry, Weizmann Institute of Science, Rehovot 76100, Israel

ABSTRACT: *Conus* venoms are estimated to comprise over 100,000 distinct pharmacologically active peptides, the majority probably targeting ion channels. Through the characterization of a cytolytic peptide from the venom of *Conus mustelinus*, conolysin-Mt, we expand the known conopeptide mechanisms to include association with and destruction of cellular membranes. A new 23AA conopeptide, conolysin-Mt has potent hemolytic activity when tested on human erythrocytes. At a concentration of 0.25 μM, the peptide permeabilized both negatively charged prokaryotic (PE:PG) and zwitterionic eukaryotic (PC: cholesterol) model membranes. The affinity constants (K_A) of conolysin-Mt for PE:PG and PC:cholesterol model membranes were $0.9 \pm 0.3 \times 10^7$ and $3 \pm 1 \times 10^7$ M^{-1}, respectively. In contrast, conolysin-Mt exhibited low antimicrobial activity (MIC > 50 μM) against two *Escherichia coli* strains, with an MIC for the Gram-positive *S. aureus* of 25−50 μM. The specificity of conolysin-Mt for native eukaryotic membranes is a novel feature of the peptide compared to other well-characterized cytolytic peptides such as melittin.

Cytolytic peptides, defined by their ability to partially or completely destroy cell membranes, are among the largest group of toxins produced by living organisms, which include bacteria, viruses, insects, marine invertebrates, and reptiles (*1*). By targeting a universal component of living cells, the lipid bilayer, cytolytic peptides can be employed for a wide range of biological interactions. Melittin is the classical cytolytic venom peptide; it is the major component in the venom of the European honey bee *Apis melifera* (*2*). The characterization of melittin has established general properties for cytolytic peptides. Melittin is an amphipathic peptide consisting of 26 amino acids. Although, in water, melittin exists as a random coiled monomer (*3*), in high salt or peptide concentrations, melittin aggregates into tetrameric complexes with defined α-helical conformations (*4−6*). The extensive characterization of melittin has made it a model for protein interactions with biological membranes (*7−10*).

A rich source of biologically active venom components are the predatory marine gastropods in the genus *Conus*. Each cone snail produces 100 to 200 different peptides, with essentially no overlap among the venoms of different *Conus* species. Thus, as a group, conopeptides comprise ca. 100,-000 different biologically active peptides within the 700 living *Conus* species. A number of these peptides have been synthesized and characterized; the vast majority of these with known molecular targets have been shown to target various types of ion channels, both ligand-gated and voltage-gated.

Surprisingly, there have been no well-characterized cytolytic peptides described from *Conus* venoms to date. In this report, we describe a peptide from the vermivorous species *Conus mustelinus* (Figure 1), and its cytolytic effect on cell membranes. This is the first conopeptide shown to have the ability to disrupt the integrity of cell membranes.

EXPERIMENTAL PROCEDURES

Materials. Egg phosphatidylcholine (PC[1]), egg phosphatidylglycerol (PG), phosphatidylethanolamine (PE) (type V, from *Escherichia coli*), cholesterol (extra pure) *N*-octyl α-D-glucopyranoside (OG), and bovine serum albumin (BSA) were purchased from Sigma. Calcein was purchased from Molecular Probes (Junction City, OR). All other reagents were of analytical grade. Buffers were prepared in double-distilled water (DDW).

Mouse IC Bioassay. Sixteen day old Swiss Webster mice (∼10 gm) were used to test the ability of *C. mustelinus* fractions to elicit prototypical dose-dependent behavioral patterns associated with alterations in CNS signaling pathways. Fractions were tested using an Ultra-fine insulin syringe at a depth no greater than 2 mm. Behavioral observations of each mouse were conducted for a total of 4 h postinjection. Deviations in the normal behavior, as compared with mice injected with only saline, were recorded with the time at which they occurred. A total of 115 mice were assayed in order to identify and characterize this peptide.

* To whom correspondence should be addressed. Tel: (801) 581-8370. Fax: (801) 585-5010. E-mail: olivera@biology.utah.edu.
[‡] University of Utah.
[§] These authors contributed equally to this work.
[‖] Weizmann Institute of Science.

[1] Abbreviations: AA, amino acid; PE, phosphatidylethanolamine; PG, phosphatidylglycerol; PC, phosphatidylcholine; IC, intracranial; MIC, minimum inhibitory concentration; OG, *N*-octyl α-D-glucopyranoside; BSA, bovine serum albumin; DDW, double-distilled water; HPLC, high performance liquid chromatography; AcN, acetonitrile; TFA, trifluoroacetic acid; SUVs, small unilamellar vesicles; LUVs, large unilamellar vesicles.
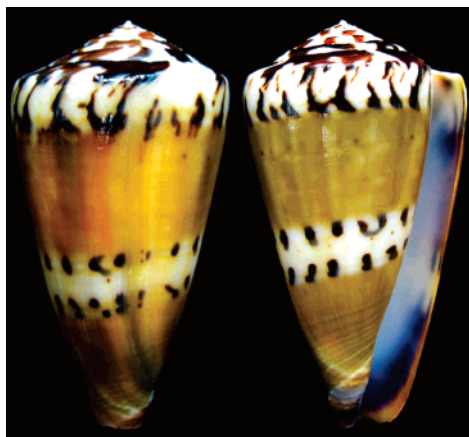
FIGURE 1: A picture of the shell of *C. mustelinus*, a vermivorous cone snail.

HPLC Purification of the Conolysin-Mt Peptide from Lyophilized Venom. A total of 200 mg of lyophilized venom from *C. mustelinus* was suspended in 2.0 mL of B45 (45% AcN:55% H$_2$O with 0.2% TFA) and mixed via sonication for 15 s, and centrifuged in a Jouan CR412 refrigerated tabletop centrifuge at 5000 rpm for 15 min. The supernatant was diluted with 0.1% TFA and applied in two separate runs onto a Discovery BIO Wide Pore C5 semipreperatory column. HPLC elution was performed using a gradient of 1.8% B90/min at a flow rate of 5.0 mL/min. All major elution peaks were collected as separate fractions. A small part of each fraction, equivalent to their proportions found in 5 mg of crude venom, was lyophilized and tested in the mouse IC bioassay. Subfractionation of the bioactive peak (denoted by an asterisk in Figure 2) identified from the mouse IC bioassay was achieved using an elution gradient of 47%−57% B90 over 30 min at a flow rate of 1.0 mL/min. A small portion of these fractions (40−200 pmol) were submitted for MALDI-TOF (courtesy of Mass Spec Facility, University of Utah). Sequence determination of the two major components within this subfractionation was completed by Edman degradation using the Applied Biosystems model 492 Sequenator (courtesy of Dr. Robert Schackmann of the DNA/ Peptide Facility, University of Utah).

Peptide Synthesis. The moonwalker peptide was synthesized using an ABI 433A peptide synthesizer (Perkin-Elmer, Foster City, Ca.). Fmoc-protected amino acids were activated with HBTU (2-(1*H*-benzotriazole-1-yl)-1,1,3,3-tetramethyluronium hexafluorophosphate) in the presence of DIEA (*N*,*N*′-diisopropylethylamine) and HOBt (1-hydroxybenzotriazole). After each coupling step, the Fmoc protecting group was removed from the amine using 20% piperidine. A small portion of the crude peptide obtained after cleavage with Reagent K (TFA:H$_2$O:thioanisole:ethanedithiol:phenol 85: 5:5:2.5:2.5) was submitted for MALDI-TOF (courtesy of Mass Spec Facility, University of Utah) to verify that the proper sequence was synthesized. The synthetic peptide was purified (>98%) using a preparatory HPLC method identical to the analytical method shown above to purify the native peptide. HPLC coelution experiments were conducted under the same conditions to verify that the native and synthetic peptides had similar physical properties.

Oocyte Whole-Cell Electrophysiological Recordings. The *Xenopus* oocyte expression system was used to study the effect of the moonwalker peptide on Kv1.3 channels. Oocyte isolation and Kv1.3 channel expression were conducted as described previously (*11*). Whole-cell currents were recorded under two-electrode voltage-clamp control using a Turbo-Tec amplifier (npi electronic, Tamm, Germany). Current records were low-pass-filtered at 1 kHz (−3 db) and sampled at 4 kHz. The bath solution was normal frog Ringer's solution (*12*) containing 115 mM NaCl, 2.5 mM KCl, 1.8 mM CaCl2, and 10 mM Hepes (pH 7.2) (NaOH). All electrophysiological experiments were performed at room temperature with a holding current of −70 mV (19−22 °C).

*Preparation of LUVs and SUVs. S*mall unilamellar vesicles (SUVs) were prepared by sonication of PC/cholesterol (9:1 w/w) or PE/PG(7:3 w/w) dispersions (*13*). Briefly, dry lipid and cholesterol (9:1 w/w) were dissolved in a CHCl$_3$/MeOH mixture (2:1 v/v). The solvents were then evaporated under a stream of nitrogen, and the lipids (at a concentration of 7.2 mg/mL) were subjected to a vacuum for 1 h and then resuspended in the appropriate buffer, by vortexing. The resultant lipid dispersions were then sonicated for 5−15 min in a bath type sonicator (G1125SP1 sonicator, Laboratory Supplies Co. Inc., Hicksville, NY) until clear. Alternatively, large unilamellar vesicles (LUVs) were prepared from PC/ cholesterol (9:1, w/w) or PE/PG (7:3 w/w) (*14*). The procedure was as follows. Dry lipids were hydrated in buffer and dispersed by vortexing to produce large multilamellar vesicles. The lipid suspension was freeze−thawed five times and then extruded eight times through polycarbonate membranes with 0.1 or 0.4 μm diameter pores (Nuclepore Corp., Pleasanton, CA).

Antimicrobial Assays. The antibacterial activity of conolysin-Mt was tested against three bacterial strains: (i) *E. coli* D21; (ii) *E. coli* ATCC 25922; and (iii) *S. aureus* ATCC 6538. Assays were conducted in sterile 96-well plates in a final volume of 100 μL as follows. 50 μL aliquots of a suspension containing bacteria (mid-log phase; 10^6 colony-forming units/mL) in LB culture medium were added to 50 μL of water containing peptide in 2-fold serial dilutions. After incubation at 37 °C for 18−20 h, inhibition of growth was determined by measuring the absorbance at 600 nm with a Microplate autoreader E3109 (Bio-tek Instruments, Winooski, VT). Antibacterial activities were expressed as the minimal inhibitory concentration at which 100% inhibition of growth was observed. All antibacterial experiments were conducted in triplicate.

Hemolytic Activity Assays. Human red blood cells (hRBCs) were used to test the hemolytic activity of conolysin-Mt. Freshly isolated hRBCs were rinsed three times with PBS (35 mM phosphate buffer, 0.15 M NaCl, pH 7.3), concentrated by centrifugation for 10 min at 800*g*, and resuspended in PBS to form a stock hRBC solution. Various concentrations of conolysin-Mt dissolved in PBS were then added to 50 μL of the stock hRBC solutions creating final volumes of 100 μL, of which the final erythrocyte concentrations were 4% v/v. The resulting suspension was incubated at 37 °C with agitation for 60 min. Incubations were centrifuged at 800*g* for 10 min, and hemoglobin release was assessed as the total absorbance of the supernatant at 540 nm. Controls for zero hemolysis (blank) and 100% hemolysis consisted of hRBCs suspended in normal PBS and 1% Triton-X 100, respectively.

Membrane Permeation Assays. Membrane permeation caused by varying concentrations of conolysin-Mt was
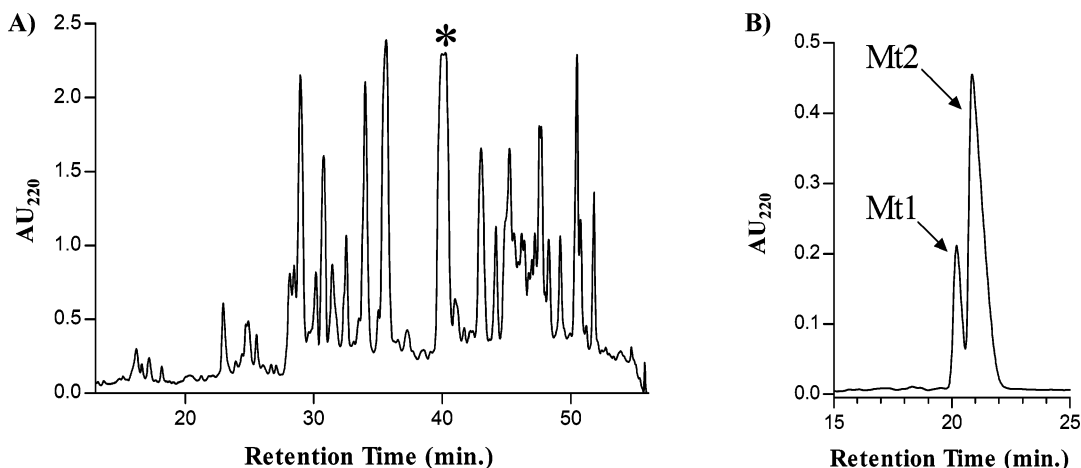
FIGURE 2: Purification of the conolysin-Mt peptide from *C. mustelinus* crude venom extract. (A) Initial HPLC fractionation of crude venom on a Discovery BIO Wide Pore C5 semipreperatory column with a linear gradient of 1.8% B90/min at a flow rate of 5.0 mL/min. The predominant bioactive fraction (43; elution time of 39.4−40.9 min) is denoted by an asterisk. (B) Analytical fractionation of 43 using a gradient of 47−57% B90 over 30 min at a flow rate of 1.0 mL/min. The moonwalker peptides isolated from each peak are indicated.

assessed utilizing the calcein release assay (*15*). Briefly, calcein (60 mM in 10 mM HEPES and 150 mM NaCl, pH 7.4; self-quenching concentration) was entrapped in SUVs composed of PC:cholesterol (9:1 w/w) or PE:PG (7:3 w/w) 10 mg/mL. Nonencapsulated calcein was removed from liposome suspensions by gel filtration using Sephadex G-50 (Pharmacia) columns connected to a low-pressure LC-system (Pharmacia). The eluents were monitored by UV absorbance ($\lambda = 280$ nm), and the peaks corresponding to intact vesicles were collected and diluted 10-fold in the same buffer. A final concentration of 2.5 μM SUVs was used in all subsequent experiments. Fluorescence was monitored at room temperature ($\lambda_{ex} = 485$ nm, $\lambda_{em} = 515$ nm). Because the calcein dye trapped inside the vesicles is self-quenching, membrane permeability is measured as a direct increase in fluorescence associated with peptide-induced calcein release. Under these experimental conditions, the absence of peptide triggered a leakage rate of less than 1% after 5 h. Dose-dependent activity was measured using peptide-to-lipid ratios in the range of 0.007−0.8. Fluorescence measurements associated with complete release of calcein (i.e., 100% activity) were obtained by SUV disruption with Triton X-100 at a final concentration of 0.1% v/v.

FTIR Spectroscopy. The spectra were obtained with a Bruker equinox 55 FTIR spectrometer equipped with a deuterated triglyceride sulfate detector and coupled to an ATR device as described previously (*16*). Briefly, a mixture of PE/PG or PC/cholesterol (0.5 mg) alone or with peptide (∼20 μg) was deposited on a ZnSe horizontal ATR prism (80 × 7 mm). The aperture angle of 45° yielded 25 internal reflections. Prior to sample preparations, trifluoroacetate (CF$_3$COO$^-$) counterions, which strongly associate with the peptides, were replaced with chloride ions through several washes with 0.1 M HCl followed by lyophilization. This washing procedure was continued until the absorption band near 1673 cm^{-1} was eliminated (*17*). Lipid−peptide mixtures were prepared by dissolution in a mixture of MeOH/CH$_2$-Cl$_2$ (1:2 v/v) and drying under a stream of anhydrous nitrogen while moving a Teflon bar back and forth along the ZnSe prism. Spectra were recorded, and the respective pure phospholipid spectra were subtracted to yield the difference spectra. The background for each spectrum was a clean ZnSe

prism. Hydration of the sample was achieved by introducing excess deuterium oxide (^{2}H$_2$O) into a chamber placed on top of the ZnSe prism in the ATR casting and incubating for 2 h before spectral acquisition. The H/D (proton to deuterium) exchange was considered complete after complete shifting of the amide II band. Any contribution of ^{2}H$_2$O vapor to the absorbance spectra near the amide I peak region was eliminated by subtracting the spectra of pure lipids equilibrated with ^{2}H$_2$O under the same conditions.

ATR-FTIR Data Analysis. Prior to curve fitting, a straight baseline passing through the ordinates at 1700 and 1600 cm^{-1} was subtracted. To resolve overlapping bands, the spectra were processed using PEAKFIT^{TM} software (Jandel Scientific, San Rafael, CA). Second-derivative spectra accompanied by 13-data point Savitsky−Golay smoothing were calculated to identify the positions of the component bands in the spectra. These wave numbers were used as initial parameters for curve fitting with Gaussian component peaks. Positions, bandwidths, and amplitudes of the peaks were varied until (i) the resulting bands shifted by no more than 2 cm^{-1} from the initial parameters, (ii) all of the peaks had reasonable half-widths (<20−25 cm^{-1}), and (iii) good agreement between the calculated sum of all of the components and the experimental spectra was achieved ($r^2 > 0.99$). The relative contents of different secondary structure elements were estimated by dividing the areas of individual peaks assigned to a specific secondary structure by the whole area of the resulting amide I band.

Aggregation in Solution. Conolysin-Mt contains a single tryptophan residue at the sixth amino acid position. Using the inherent differences in Trp (6) emission characteristics between the solvent accessible state and buried oligomeric state, we compared the aggregation state of the peptides in DDW and in PBS by following the emission changes in Trp (6) through increasing peptide concentrations. Emission changes were measured using an SLM-AMINCO spectrometer ($\lambda_{ex} = 280$ nm; $\lambda_{em} = 330$ nm; sesnsitivity-900 v; slit-8).

RESULTS

A Stereotypical Behavior Induced in the Mouse as a Bioassay. Intracranial (IC) injections of mice (*18*) have been

used to explore the pharmacological diversity of *Conus* venoms for the last 25 years; the venom peptides elicit strikingly diverse phenotypic responses that correlate with their molecular targets (*19*). In this study, crude venom extracts from nine different cone snail species were screened using the IC injection assay and a novel behavioral phenotype was discovered, different from those previously recorded in the literature. We refer to this as the "moonwalker" phenotype. The moonwalker activity was most consistently found in venom extracts from *C. mustelinus*, and the moonwalker bioassay was used to guide purification. When introduced into the CNS of 16 day old Swiss-Webster mice, the active venom fractions caused mice to shuffle backward until they encountered an obstacle, at which time the mouse would jump into the air and often go into a seizure. The backward shuffle was reminiscent of a pop star's signature dance maneuver ("the moonwalk"). When injected at concentrations equivalent to 10 mg of crude venom, 100% of the mice injected with fractions containing the moonwalker peptide displayed the moonwalker response within 2 h postinjection.

Purification and Biochemical Characterization of the Moonwalker Activity. Initial semipreparatory HPLC fractionation of *C. mustelinus* crude venom extract (Figure 2A) was carried out, and 53 fractions were collected. One fraction (43; eluted between 39.4 and 40.9 min) was found to elicit the moonwalker phenotype. MALDI-TOF analysis of fraction 43 suggested that this fraction contained only two peptides with MH^+/z values of 2692.45 and 2750.40; this data suggested that the two peptides might differ only by a glycine residue. In order to resolve the two peptides, HPLC elution had to be carried out at 45 °C (Figure 2B); the two peptides were found in a ratio of 1:4. MALDI-TOF analyses of the two subfractions confirmed that the two peptides had been resolved.

When tested using the mouse IC bioassay, both elicited the moonwalker phenotype with varying efficacy. The less abundant of the two peptides was more active in this assay, causing the full moonwalker phenotype to be observed within ~35 min using roughly 3 nmol of peptide ($n = 1$ in five separate experiments); the more abundant peptide elicited the phenotype in ~150 min, using roughly 12 nmol ($n = 1$ in five separate experiments).

Primary amino acid sequence determination using automated Edman degradation confirmed that the two peptides were related, having the following sequences:

FHPSLWVLIPQYIQLIRKILKSG

(for the less abundant peptide, Mt1)

FHPSLWVLIPQYIQLIRKILKS

(for the other peptide, Mt2)

The calculated mass average (2750.4) of Mt1 matched the observed mass (2750.4) exactly. The glycine residue mentioned earlier was found at the C-terminus of this peptide. Mass spectroscopy data of the more abundant peptide (2692.45) differed from the calculated average mass (2693.3) by ~1 mass unit. When combined with known posttranslational modifications of conopeptides, the data suggests that the most abundant peptide found in *C. mustelinus* venom with the moonwalker activity is C-terminally amidated.

The more active peptide, Mt1, was synthesized for further characterization. The synthetic material both coeluted with
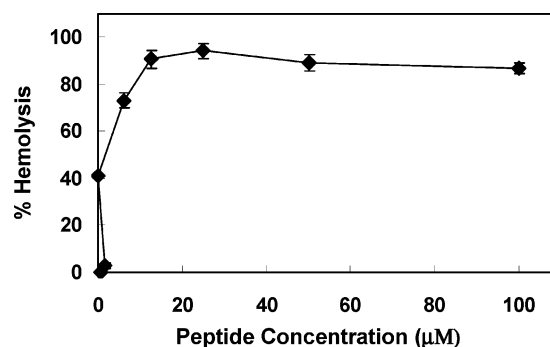

FIGURE 3: Dose response of the hemolytic activity of the conolysin-Mt toward 4% hRBCs. The % hemolysis was calculated as the ratio between the supernatant absorbance at 540 nm and the absorbance of hRBCs treated with 1% Triton (100% hemolysis). Similar results were reported by others for melittin and D-melittin (*20*, *21*).

the native peptide and elicited the same phenotypic response in the mouse IC bioassay ($n = 1$ in three separate experiments). Four additional mice were injected with the synthetic peptide (0.5, 1, 2, and 5 nmol, respectively) for an initial dose–response analysis. When injected into the CNS of 17 day old mice, 2 nmol of the synthetic peptide was sufficient to elicit the moonwalker phenotype (data not shown).

Physiological Characterization of the Moonwalker Peptide. Our initial working hypothesis was that the peptides with moonwalker activity were excitotoxins, and the synthetic peptide was tested on *Xenopus* oocytes expressing cloned potassium channels. It became apparent that the peptide potently disrupted oocyte membranes. Within seconds after peptide application, the membrane potential of oocytes collapsed ($n = 4$). Within minutes, there were visible holes in the oocytes (at 60× magnification), with yolk leaking out into the surrounding medium. This revealed that the peptide causing the moonwalker phenotype was in fact a cytolytic toxin.

The peptide was tested for both antibacterial and hemolytic efficacy; it exhibited low antibacterial activity against the two *E. coli* strains tested, with minimal inhibitory concentration (MIC) >50 μM. The MIC against the Gram-positive *S. aureus* was 25–50 μM. In comparison, melittin has potent antibacterial activity on both Gram-negative and Gram-positive bacteria. Its antibacterial activity under the same assay conditions is ~1 μM to 20 μM depending upon the bacterial strain used (*20–22*). In contrast, the peptide showed very high hemolytic activity against hRBCs (40% hemolysis at 1 μM; ~90% at 10 μM) (Figure 3). The hemolytic activity of the peptide was equipotent with melittin in causing complete lyses of hRBCs (*20–22*). The hemolytic activity of the moonwalker peptide, coupled with its effects on *Xenopus* oocytes, establishes its cytolytic activity. This peptide thus defines a new class of cytolytic *Conus* peptides that we designate as "conolysins;" the conolysin from *C. mustelinus* is designated conolysin-Mt.

Conolysin-Mt Permeabilized Both Prokaryotic and Eukaryotic Model Membranes. Conolysin-Mt was tested for the ability to permeabilize negatively charged prokaryotic (PE: PG) and zwitterionic eukaryotic (PC:cholesterol) model membranes by following the changes in calcein emission upon release from model membrane small unilamellar vesicles (SUVs). Conolysin-Mt induced complete release of
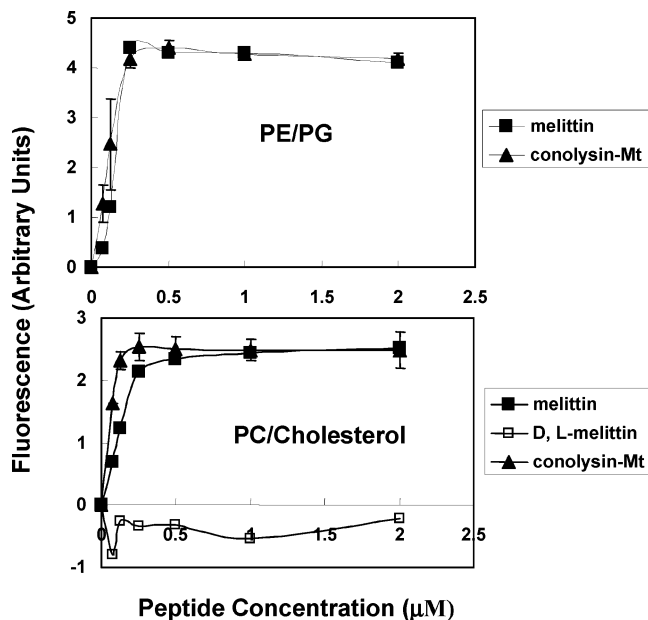
FIGURE 4: Calcein release induced by conolysin-Mt added to SUVs composed of PE/PG (7:3) (upper panel) and PC/cholesterol (9:1) (lower panel) phospholipids encapsulating calcein (2.5 μM final concentration).
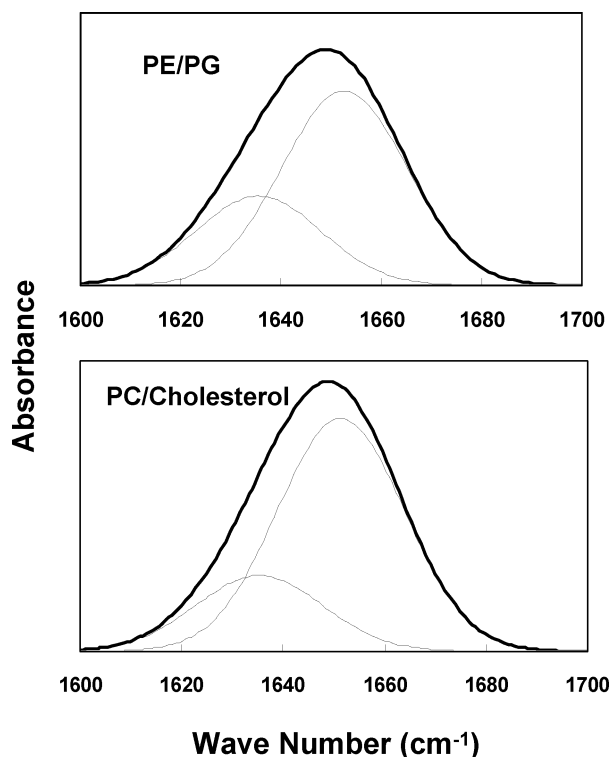

Wave Number (cm⁻¹)

FIGURE 5: FTIR spectra deconvolution of the fully deuterated amide I band (1600–1700 cm⁻¹) of conolysin-Mt in PE:PG (7:3 w/w) or PC:cholesterol (9:1 w/w) multibilayers. The component peaks are the result of curve fitting using a Gaussian line shape. The sums of the fitted components superimpose on the experimental amide I region spectra. Bold lines represent the experimental FTIR spectra after Savitzky–Golay smoothing; the thin lines represent the fitted components. A 120:1 lipid/diastereomer molar ratio was used.

calcein from both prokaryotic and eukaryotic model membranes at 0.25 μM (Figure 4). Analyses using the nonlinear least-squares (NLLSQ) demonstrated that the affinity constants (K_A) of the peptide were similar for both PE:PG and PC:cholesterol model membranes ($0.9 \pm 0.3 \times 10^7$ and $3 \pm$

Table 1: Peptide Structure as Determined by ATR-FTIR Spectroscopy from the Deconvolution of the Amide I Bands of the All-L and the Diastereomeric Peptides Incorporated into LPS Multibilayers

membrane type	α-helix (%)	aggregated β-strand
PE:PG	68.1 ± 4.1	31.9 ± 4.1
PC:cholesterol	75.1 ± 3.4	24.9 ± 3.4

Table 2: The Ability of the Peptides To Disrupte Lipid Acyl Chains as Obtained by Polerized FTIR

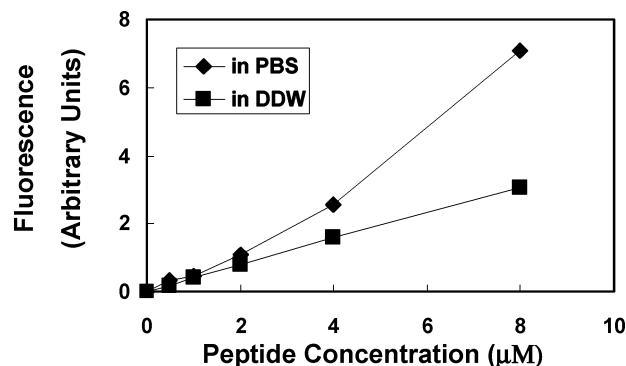|	PC:cholesterol	PC:cholesterol + peptide	PE:PG	PE:PG + peptide
$V_{antisymmetric}$ (CH₂)	1.14	1.16	1.16	1.33

FIGURE 6: The changes in the emission of natural Trp residue in PBS and in DDW. The changes in the Trp emission correlate with the peptide aggregative state, since Trp tend to quench upon oligomerization.

1×10^7 M⁻¹, respectively). Conolysin-Mt was observed to have similar activities compared to melittin, although it is slightly more active on PE:PG compared to melittin which was tested in parallel experiments (Figure 4).

The Structure of Conolysin-Mt within Prokaryotic and Eukaryotic Model Membranes. FTIR spectroscopy was used to determine the secondary structure of the peptides within both phospholipid model membranes. The results suggested that conolysin-Mt adopted a predominantly α-helical structure with a small portion of aggregated β-sheet in both prokaryotic and eukaryotic model membranes (Figure 5). The relative areas of the component peaks, derived from the data in Figure 5B, are summarized in Table 1.

The ability of the peptide to disrupt the lipid acyl chains was evaluated by using polarized ATR-FTIR spectroscopy. The symmetric (ν_{sym}(CH₂) $\approx$2853 cm⁻¹) and the antisymmetric (ν_{sym}(CH₂) $\approx$2922 cm⁻¹) vibrations of lipid methylene C–H bonds are perpendicular to the molecular axes of fully extended hydrocarbon chains. Thus, measuring the dichroism of infrared light absorbance can reveal the order of the membrane sample relative to the prism surface. The effect of the peptide on the acyl chain order was estimated by comparing the CH₂ stretching dichroic ratio of phospholipid multibilayers alone with that obtained of lipid-bound peptides (see Table 2). The calculated values (R) based on the antisymmetric vibrations revealed that conolysin-Mt had a strong effect on PE:PG acyl chains while on PC:cholesterol it had a moderate effect.

Conolysin-Mt aggregation was assessed by following the changes in Trp (6) emission at different concentrations of

A)
```
melittin        GIGAVLKVLTTGLPALISWIKRKRQQ- 26
conolysin-Mt    -FHPSLWVL---IPQYIQLIRKILKSG 23
                :  .  *  **    :*   *.  *::   :.
```

```
retro-melittin  QQRKRKIWSILAPLGTTLVKLVAGIG 26
conolysin-Mt    --FHPSLW-VLIPQYIQLIRKILKSG 23
                :  .:*  :*  *      *::  :     *
```

B)

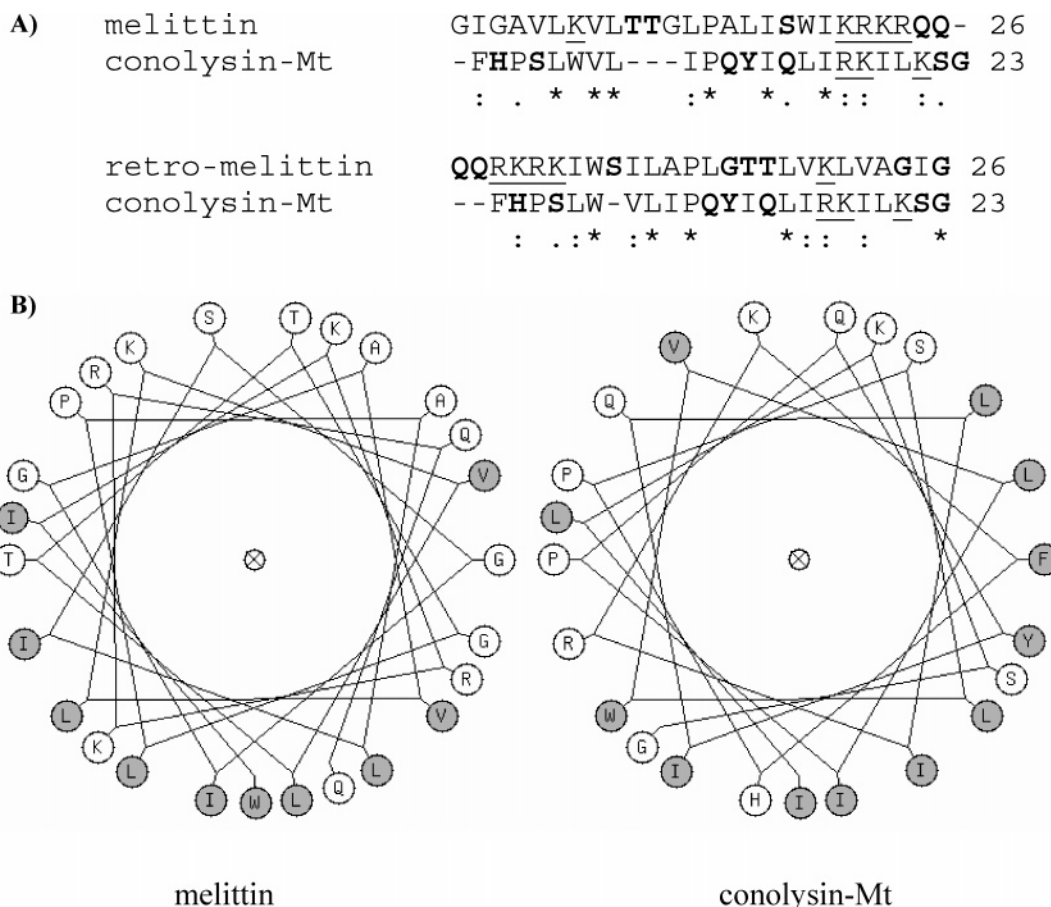melittin   conolysin-Mt

FIGURE 7: Comparisons of homology between melittin and conolysin-Mt. The primary amino acid sequence alignment using ClustalW (A) illustrates that conolysin-Mt shares 26% homology in direct amino acid sequence (asterisks), 47.8% homology in terms of conservative substitutions (colons), and 60.8% in terms of semiconservative substitutions with melittin (dots). Charged residues are underlined, and uncharged hydrophilic residues are bolded. The helical wheel diagrams (B) of melittin and conolysin-Mt created using Kael's Helical Wheel Applet (http://kael.net/helical.htm) also shows the conservation of amphipathicity between the two peptides. Polar residues are shown in white, and hydrophobic residues are shown in gray.

the peptide. In buffer (PBS) the changes were higher compared with DDW and were cooperative (Figure 6), indicating that the conolysin-Mt tended to aggregate in solutions with moderate ionic strength, but not in deionized water.

DISCUSSION

Conus venom peptides have proven to be diverse not only in sequence but also in the underlying biochemical mechanisms through which they exert their physiological effects (*23*). Because the venom peptides are directly translated gene products, it has been suggested that the peptide diversity observed in the venom of particular *Conus* species is a direct consequence of the accelerated evolution of these genes in response to diverging biotic interactions in different species (*24*, *25*). In this study, we characterize a new mechanism of action for conopeptides: conolysin-Mt, isolated and characterized from the venom of *C. mustelinus*, is a cytolytic peptide that destroys the integrity of biological membranes. To our knowledge, this is the first demonstration that a peptide derived from *Conus* venoms is cytolytic.

Comparisons between the primary amino acid sequences of melittin and conolysin-Mt using the amino acid sequence homology program ClustalW (EBI Tools), although arising through convergent evolution, suggest that conolysin-Mt has similarities to the C-terminal α-helix of melittin (Figure 7).

This C-terminal region includes about 2/3 of conolysin-Mt amino acids, which is in agreement with about 60%−70% α-helical content in membranes as determined by FTIR spectroscopy (Figure 5, Table 1). The N-terminus of the toxin which contains two proline residues is probably the β-sheet component (FTIR spectroscopy). The similarities between the peptides combined with the FTIR studies suggest that conolysin-Mt might also have a hinge at proline in position 10 between the C-helix and the rest of the molecule. However, if one compares the helical wheel diagrams of conolysin-Mt vs melittin, it becomes apparent that the orientation of conolysin-Mt monomers within the conolysin-Mt aggregates might be almost completely opposite of the orientation observed for melittin monomers, an orientation that could more readily be compared to a synthetic analogue, retro-melittin (*8*). Although not tested here, it has been shown that the lytic activity of retro isomers of membrane active lytic peptides, including melittin, is similar to that of their parental peptides (*20*, *21*, *26*, *27*).

Conolysin-Mt differs functionally from melittin, the model cytolytic peptide, in that it is not antibacterial (see Figure 7 for a comparison between the two peptides). In order to better understand the basis for differences in the antibacterial and hemolytic activities of this peptide, we tested its ability to permeabilize negatively charged prokaryotic (PE:PG) and zwitterionic eukaryotic (PC:cholesterol) model membrane

SUVs. Conolysin-Mt permeabilized both types of SUVs, and since these systems reach equilibrium at definable peptide concentrations, we were able to calculate the affinity constants of the peptide for both model membranes; the association constants were determined to be $0.9 \pm 0.3 \times 10^7$ and $3 \pm 1 \times 10^7$ M^{-1} for PE:PG and PC:cholesterol model membranes, respectively.

The ability of conolysin-Mt to disrupt the lipid acyl chains was further evaluated using polarized ATR-FTIR spectroscopy. Conolysin-Mt had a strong effect on PE:PG acyl chains while on PC:cholesterol it had a moderate effect suggesting that although the peptide is potent in permeabilizing both model membranes, the mechanism by which it disrupts these membranes might be different. We note that melittin has been proposed to elicit its effects on prokaryotic and eukaryotic membranes via two separate mechanisms. Thus, conolysin-Mt acts to potently disrupt SUVs composed of prokaryotic and/or eukaryotic membrane components at concentrations similar to those of melittin (see Figure 4) even though it does not act as an antibacterial peptide. The observed differences in antibacterial vs hemolytic activities of conolysin-Mt differentiate it from melittin. Studies using small unilamellar vesicles and solid-state ^{13}C nuclear magnetic resonance suggest that melittin forms distinct membrane spanning pores (6, 28−32), while in negatively charged membranes, melittin acts through a classical carpet mechanism (31, 33). There may be intrinsic differences in mechanism between melittin and conolysin-Mt. Alternatively, the presence of a capsule (cell wall), which shrouds the bacteria, may prevent the peptide from reaching the bacterial membrane when in its aggregated state. Like melittin, conolysin-Mt has a propensity to aggregate in buffered solutions, but remains as a random monomer in deionized water. The size of the aggregates increases with an increase in the concentration of the peptide as indicated in the positive curvature of the tryptophan fluorescence upon increasing the peptide concentration (Figure 6). Larger aggregates might fail to pass the outer barrier of bacteria, accounting for why conolysin-Mt exhibits low antibacterial activity. In agreement with that is our finding that the peptide is more active against Gram-positive rather than Gram-negative bacteria, as the latter has an additional outer membrane. However, these aggregates still can access the erythrocyte membrane and, thus, retain their hemolytic activity. Further studies of the biophysical mechanisms of conolysin-Mt need to be conducted in order to more fully explain the observed differences in the ability of conolysin-Mt to act as a hemolytic and antibacterial peptide. In light of the extensive studies carried out to understand melittin activity, we suggest that conolysin-Mt might be useful in identifying determinants in cytolytic peptides that define specificity toward prokaryotic and eukaryotic targets.

REFERENCES

1. Alouf, J. E. (2001) Pore-forming bacterial protein toxins: An overview, *Curr. Top. Microbiol. Immunol. 257*, 1−14.

2. Habermann, E. (1972) Bee and wasp venoms, *Science 177*, 314−322.

3. Lauterwein, J., Brown, L. R., and Wuthrich, K. (1980) High-resolution ^1H-NMR studies of monomeric melittin in aqueous solution, *Biochim. Biophys. Acta 622*, 219−230.

4. Talbot, J. C., Dufourcq, J., de Bony, J., Faucon, J. F., and Lussan, C. (1979) Conformational change and self association of monomeric melittin, *FEBS Lett. 102*, 191−193.

5. Tatham, A. S., Hider, R. C., and Drake, A. F. (1983) The effect of counterions on melittin aggregation, *Biochem. J. 211*, 683−686.

6. Brown, L. R., Lauterwein, J., and Wuthrich, K. (1980) High-resolution ^1H-NMR studies of self-aggregation of melittin in aqueous solution, *Biochim. Biophys. Acta 622*, 231−244.

7. DeGrado, W. F., Musso, G. F., Lieber, M., Kaiser, E. T., and Kezdy, F. J. (1982) Kinetics and mechanism of hemolysis induced by melittin and by a synthetic melittin analogue, *Biophys. J. 37*, 329−338.

8. Juvvadi, P., Vunnam, S., and Merrifield, R. B. (1996) Synthetic melittin, its enantio, retro, and retroenantio isomers, and selected chimeric analogs: Their antibacterial, hemolytic, and lipid bilayer action, *J. Am. Chem. Soc. 118*, 8989−8997.

9. Perez-Paya, E., Houghten, R. A., and Blondelle, S. E. (1995) The role of amphipathicity in the folding, self-association and biological activity of multiple subunit small proteins, *J. Biol. Chem. 270*, 1048−1056.

10. Beschiaschvili, G., and Seelig, J. (1990) Melittin binding to mixed phosphatidylglycerol/phosphatidylcholine membranes, *Biochemistry 29*, 52−58.

11. Jacobsen, R. B., Koch, E. D., Lange-Malecki, B., Stocker, M., Verhey, J., Van Wagoner, R. M., Vyazovkina, A., Olivera, B. M., and Terlau, H. (2000) Single amino acid substitutions in kappa-conotoxin pviia disrupt interaction with the shaker k+ channel, *J. Biol. Chem. 275*, 24639−24644.

12. Horton, R. M., Manfredi, A. A., and Conti-Tronconi, B. M. (1993) The 'embryonic' gamma subunit of the nicotinic acetylcholine receptor is expressed in adult extraocular muscle, *Neurology 43*, 983−986.

13. Gazit, E., Lee, W. J., Brey, P. T., and Shai, Y. (1994) Mode of action of the antibacterial cecropin b2: A spectrofluorometric study, *Biochemistry 33*, 10681−10692.

14. Kliger, Y., Aharoni, A., Rapaport, D., Jones, P., Blumenthal, R., and Shai, Y. (1997) Fusion peptides derived from the hiv type 1 glycoprotein 41 associate within phospholipid membranes and inhibit cell-cell fusion. Structure-function study, *J. Biol. Chem. 272*, 13496−13505.

15. Allen, T. M., and Cleland, L. G. (1980) Serum-induced leakage of liposome contents, *Biochim. Biophys. Acta 597*, 418−426.

16. Oren, Z., and Shai, Y. (1996) A class of highly potent antibacterial peptides derived from pardaxin, a pore-forming peptide isolated from moses sole fish pardachirus marmoratus, *Eur. J. Biochem. 237*, 303−310.

17. Surewicz, W. K., Mantsch, H. H., and Chapman, D. (1993) Determination of protein secondary structure by fourier transform infrared spectroscopy: A critical assessment, *Biochemistry 32*, 389−394.

18. Clark, C., Olivera, B. M., and Cruz, L. J. (1981) A toxin from the venom of the marine snail conus geographus which acts on the vertebrate central nervous system, *Toxicon 19*, 691−699.

19. Olivera, B. M., McIntosh, J. M., Clark, C., Middlemas, D., Gray, W. R., and Cruz, L. J. (1985) A sleep-inducing peptide from conus geographus venom, *Toxicon 23*, 277−282.

20. Bessalle, R., Kapitkovsky, A., Gorea, A., Shalit, I., and Fridkin, M. (1990) All-d-magainin: Chirality, antimicrobial activity and proteolytic resistance, *FEBS Lett. 274*, 151−155.

21. Wade, D., Boman, A., Wahlin, B., Drain, C. M., Andreu, D., Boman, H. G., and Merrifield, R. B. (1990) All-d amino acid-containing channel-forming antibiotic peptides, *Proc. Natl. Acad. Sci. U.S.A 87*, 4761−4765.

22. Oren, Z., and Shai, Y. (1997) Selective lysis of bacteria but not mammalian cells by diastereomers of melittin: Structure-function study, *Biochemistry 36*, 1826−1835.

23. Terlau, H., and Olivera, B. M. (2004) Conus venoms: A rich source of novel ion channel-targeted peptides, *Physiol. Rev. 84*, 41−68.

24. Olivera, B. M. (2002) Conus venom peptides: Reflections from the biology of clades and species, *Annu. Rev. Ecol. Syst. 33*, 25−47.

25. Olivera, B. M. (2006) Conus peptides: Biodiversity-based discovery and exogenomics, *J. Biol. Chem. 281*, 31173−31177.

26. Papo, N., and Shai, Y. (2003) New lytic peptides based on the d,l-amphipathic helix motif preferentially kill tumor cells compared to normal cells, *Biochemistry 42*, 9346−9354.

27. Merrifield, R. B., Juvvadi, P., Andreu, D., Ubach, J., Boman, A., and Boman, H. G. (1995) Retro and retrosenantio analogs of cecropin-melittin hybrids, *Proc. Natl. Acad. Sci. U.S.A. 92*, 3449−3453.

28. Park, S. C., Kim, J. Y., Shin, S. O., Jeong, C. Y., Kim, M. H., Shin, S. Y., Cheong, G. W., Park, Y., and Hahm, K. S. (2006) Investigation of toroidal pore and oligomerization by melittin using transmission electron microscopy, *Biochem. Biophys. Res. Commun. 343*, 222−228.

29. Smith, R., Separovic, F., Milne, T. J., Whittaker, A., Bennett, F. M., Cornell, B. A., and Makriyannis, A. (1994) Structure and orientation of the pore-forming peptide, melittin, in lipid bilayers, *J. Mol. Biol. 241*, 456−466.

30. Ladokhin, A. S., Selsted, M. E., and White, S. H. (1997) Sizing membrane pores in lipid vesicles by leakage of co-encapsulated markers: Pore formation by melittin, *Biophys. J. 72*, 1762−1766.

31. Papo, N., and Shai, Y. (2003) Exploring peptide membrane interaction using surface plasmon resonance: Differentiation between pore formation versus membrane disruption by lytic peptides, *Biochemistry 42*, 458−466.

32. Rex, S., and Schwarz, G. (1998) Quantitative studies on the melittin-induced leakage mechanism of lipid vesicles, *Biochemistry 37*, 2336−2345.

33. Ladokhin, A. S., and White, S. H. (2001) 'Detergent-like' permeabilization of anionic lipid vesicles by melittin, *Biochim. Biophys. Acta 1514*, 253−260.